Molecular Crystals and Liquid Crystals Science and Technology. Section A. Molecular Crystals and Liquid Crystals

Publication details, including instructions for authors and subscription information:
http://www.tandfonline.com/loi/gmcl19

X-Ray Scattering and Thermal Characterization of α,β-Dimethyl Stilbene Polycarbonates

Yao-Yi Cheng [a], Peggy Cebe [a], Malcolm Capel [b], Heidi Schreuder-gibson [c], Aaron Bluhm [c], John Stapler [c] & Walter Yeomans [c]

[a] Department of Physics and Astronomy, Tufts University, Medford, MA, 02155

[b] Biology Department, Brookhaven National Laboratory, Upton, NY, 1197

[c] U.S. Army Natick Research, Development and Engineering Center Natick, MA, 01760

Version of record first published: 24 Sep 2006.

To cite this article: Yao-Yi Cheng , Peggy Cebe , Malcolm Capel , Heidi Schreuder-gibson , Aaron Bluhm , John Stapler & Walter Yeomans (1996): X-Ray Scattering and Thermal Characterization of α,β-Dimethyl Stilbene Polycarbonates, Molecular Crystals and Liquid Crystals Science and Technology. Section A. Molecular Crystals and Liquid Crystals, 287:1, 183-203

To link to this article: http://dx.doi.org/10.1080/10587259608038755

Mol. Cryst. Liq. Cryst., 1996, Vol. 287, pp. 183–203
Reprints available directly from the publisher
Photocopying permitted by license only

X-Ray Scattering and Thermal Characterization of α,β-Dimethyl Stilbene Polycarbonates

YAO-YI CHENG[1], PEGGY CEBE[1]*, MALCOLM CAPEL[2], HEIDI SCHREUDER-GIBSON[3], AARON BLUHM[3], JOHN STAPLER[3] and WALTER YEOMANS[3]

[1]*Department of Physics and Astronomy, Tufts University, Medford, MA 02155*
[2]*Biology Department, Brookhaven National Laboratory, Upton, NY 11973*
[3]*U.S. Army Natick Research, Development and Engineering Center Natick, MA 01760*

(Received May 15, 1995; in final form November 13, 1995)

Structural and thermal characterization is reported for a series of recently synthesized[1] liquid crystalline polycarbonates based on di-methyl substituted stilbene mesogen and methylene-containing flexible spacer of length n. In this work, we focus on the α, β-dimethyl stilbene (DMS-*n*) polycarbonates and on the comparison between them and α-methyl stilbene (HMS-*n*) polycarbonates[2-4], especially those with heptane spacer. Wide angle X-ray scattering patterns show that DMS polycarbonates are able to form a nematic liquid crystalline phase. However, the liquid crystalline phase is generally not stable with respect to the crystalline phase. In the DMS polycarbonates, no distinct isotropic-to-nematic (i $\longrightarrow$ lc) transition is seen either by polarizing optical microscopy or by differential scanning calorimetry (DSC). We suggest that the steric effect of the second lateral substituent results in a less stable, virtual mesophase. For DMS-*n*, an odd-even effect is observed in the crystallization and melting temperatures for n values between four and eight. The transition temperatures associated with even parity *n* ($n = 4,6,8$) are greater than those for odd parity *n* ($n = 5,7,9$) and all transition temperatures drop when n exceeds eight. Small angle X-ray scattering studies were performed on the DMS polycarbonates to examine the structure of the crystalline phase. For *n* in the range from 5–8, DMS polycarbonates generally have higher values of linear crystallinity and crystal thickness than corresponding HMS polycarbonates.

1. INTRODUCTION

A series of polycarbonate liquid crystalline polymers (LCPs) has been synthesized[1] based on the stilbene mesogen, mono- or di-substituted with methyl groups. These polycarbonates are referred as HMS-*n* and DMS-*n*, respectively. Chemical structures of these polymers are shown below:

*To whom correspondence should be addressed.

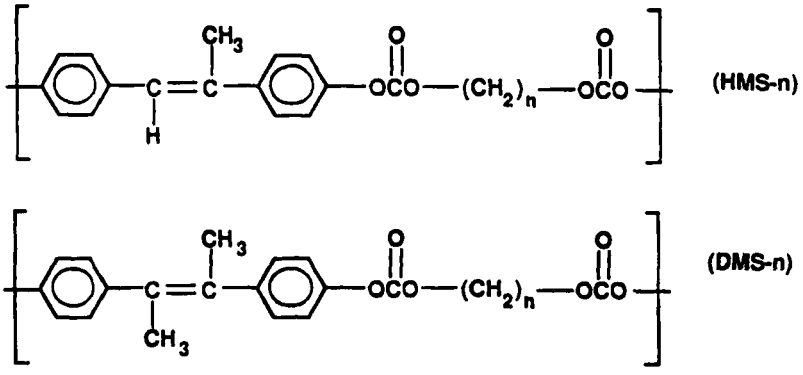

The polycarbonates with heptane flexible spacer ($n = 7$) were chosen for comparison of the effect of different mesogen substitution on their properties[1]. Polycarbonates with either mono- or di-methyl substituted stilbene mesogen (HMS-7 and DMS-7) are semicrystalline and appear to form nematic mesophases when examined using wide angle X-ray scattering[1,3]. This work concentrates on the characterization of DMS-*n* for flexible spacer number ranging from $n = 4$–10, 12. Also, the comparison between HMS and DMS polycarbonates is discussed, especially for those with the heptane flexible spacer.

Other stilbene-based LCPS, α-methyl stilbene polyethers[5] and α-methyl stilbene polyesters[6,7], were found to form an enantiotropic liquid crystalline phase in which the liquid crystalline phase is seen reversibly in heating and cooling. However, as described in our previous work[2], we found that α-methyl stilbene polycarbonates actually can only from monotropic liquid crystalline phases. The flexibility of the carbonate linkage causes the liquid crystalline phase to be less stable compared with the crystalline phase and the isotropic phase. Also, fast crystallization results from the improved intermolecular interaction attributed to the carbonate dipole[2,3]. Faster crystallization from a smectic mesophase has recently been reported by Zachman *et al.*[8]

Unlike the enantiotropic LCPs[5-7], in our monotropic α-methyl stilbene polycarbonates, HMS-*n*, the odd-even effect is barely observed in the thermal transition temperatures[2]. In these LCPs, rapid crystallization results in formation of imperfect crystals which reorganize and melt to give broad, complex endotherms. However, in HMS-*n*, an odd-even effect is clearly seen both in the lattice parameters obtained from WAXS[3] and in crystal thickness and linear crystallinity obtained from SAXS[4]. Variation in the position of the neighboring carbonate dipoles on an α-methyl stilbene polycarbonate chain, caused by parity in the flexible spacer, does affect structural organization at the unit cell level[3] and also at the level of the crystals[4].

It is believed that the insertion of bulky substituents on the mesogen will lower the stability of the liquid crystalline phase because of the steric effect[9-17]. For example, α, β-dimethyl stilbene polyesters do not have an enantiotropic liquid crystalline phase while α-methyl stilbene polyesters do[5,9,16]. In this work, we show that DMS polycarbonates do only have a virtual liquid crystalline phase. However, the odd-even effect in the crystallization and melting transition temperatures is seen

clearly in DMS-*n* for *n* ranging from four to eight. The effect of the second lateral substituent on the stilbene mesogen on the crystallization behaviour and crystalline structure is also investigated.

2. EXPERIMENTAL SECTION

2.1. Materials

The synthesis of DMS polycarbonates[1] followed the method of Sato[18]. The resultant LCPs were soluble in chloroform and obtained as fine white powders. Elemental analysis was used to verify the synthetic product[1]. All polymers studied here have reasonably high molecular weight, in the range from $M_w \sim 14{,}200$, to 32,800 with distributions (M_w/M_n) ranging from 1.8 up to 2.9[1]. For HMS-7 the degree of polymerization (dp) was 51, while for DMS-7 the dp was 36. FTir was used to verify the chemical structure.

Using molecular modeling of the chemical structures cross sectional dimensions of the mesogens were determined. The cross section of the dimethyl substituted stilbene (DMS) mesogen was found to be 8.6 Å, while the cross section of the mono-methyl substituted stilbene (HMS) mesogen was significantly smaller at 6.5Å.

2.2. X-ray Scattering

A Rigaku RU-300 rotating anode X-ray generator was used to examine films of DMS-7 in wide angle X-ray scattering (WAXS) studies using $\theta/2\theta$ reflection mode. The diffractometer has a diffracted beam graphite monochromator. Copper K_α radiation was used ($\lambda = 1.54$ Å) with a step scan interval of 0.1 degree, at a rate of 1 degree/minute, over the 2θ range from 3 to 53 degrees. Powder was dissolved in chloroform and several drops of the solution were placed onto quartz substrates. The thin films were run "as-is" without any other thermal treatment.

WAXS was also performed at room temperature using a Philips PW 1830 X-ray generator operated at 45 kV and 45 mA with Ni-filtered CuK_α radiation, and a Statton camera. The sample to film distance is calibrated using Si powder reference standard (from National Institute of Standards & Technology) rubbed on the sample surface. HMS-7 and DMS-7 fibers were hand drawn from the mesophase using tweezers. This fiber cooled rapidly in air, and will be referred to as raw fiber. Raw fiber was subsequently annealed below the melting temperature. CERIUS™, a commercial software package distributed by Molecular Simulations Inc., was used to assist in indexing of experimental X-ray diffraction patterns and determination of the crystal structure.

The X12B beam line at Brookhaven National Synchrotron Light Source (NSLS) was used to obtain small angle X-ray scattering (SAXS) data in transmission mode. For high temperature work, a Mettler hot stage was supported in the X-ray beam path by an aluminium holder, and the beam passed through the sample, which was sealed between two pieces of Kapton™ tape. A gas-filled two-dimensional histogramming wire detector was used. For isotropic samples, circular integration of the

intensity was used to enhance the signal to noise ratio. The beam profile was treated according to pinhole geometry. SAXS data were taken on two separate trips. The sample to detector distance was 1.39 m or 1.85 m, and was calibrated by cholesterol myristate and collagen fiber. X-ray wavelength was 1.38 Å or 1.53 Å.

SAXS scans at room temperature were taken for DMS-5 to 8, which were non-isothermally crystallized by cooling at 5 °C/min from the melt to room temperature. Real-time SAXS data were taken for an isothermal crystallization study. Samples were melted at 190 °C for 2.5–3 minutes, then cooled at 20 °C/min to 124 °C and held there until crystallization was finished. Data were collected during cooling from 170 to 140 °C and during the whole isothermal crystallization process. The data collection time interval was 10 seconds.

Lorentz corrected SAXS intensity, Is^2 (where s is the scattering vector, $s = 2\sin\theta/\lambda$) was also corrected for background, sample absorption, variation of incident beam intensity and thermal density fluctuation. The slope of Is^4 versus s^4 was used to get the diffraction intensity contribution from thermal density fluctuations[19,20]. The corrected intensity is used for quantitative analysis.

2.3. Thermal Properties Using Calorimetry and Optical Microscopy

Thermal properties of materials were studied using a Perkin-Elmer DSC-4 or DSC-7. Indium was used to calibrate the temperature and the heat of fusion. The studies that were done included heating and cooling at fixed rates, and isothermal crystallization to test the effect of crystallization temperature on both crystallization time and melting temperature. All scans are normalized on a per unit mass basis. All thermograms have had instrumental baseline subtraction performed. However, data were taken over several months using different initial y-axis scales, and baseline drift is apparent in some thermograms. This drift was further exacerbated in a few scans when vertical scale expansion was employed to allow several scans to be presented together for comparison with the same y-axis scaling.

Elevated temperature polarizing optical microscopy (POM) was used to study the appearance and disappearance of birefringence. Samples were cooled from the melt at 10 °C/min and the temperature of first occurrence of birefringence was recorded by visual observation. Samples were then heated at the same rate and the last occurence of birefringence was recorded.

3. RESULTS

3.1. Thermal Transition from DSC and POM

In the DSC cooling scan of DMS-4-10 and 12 cooling from the melt, usually a broad exotherm with a low temperature tail is observed, as shown in Figure 1a. In the reheating scan shown in Figure 1b, a broad endotherm with a low temperature tail caused by the melting of less perfect crystals is usually observed for most DMS samples. Tilted baselines are seen in some traces in Figure 1. These thermograms have already had instrumental baseline subtraction performed, but the baseline drift

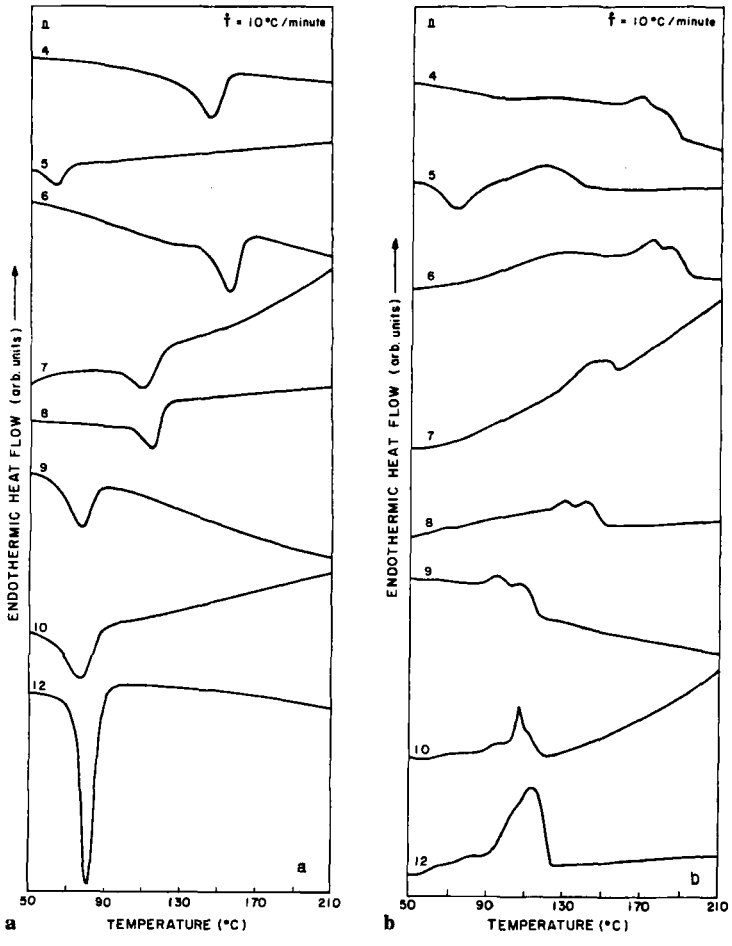

FIGURE 1 DSC thermograms of DMS-4-10, 12 at 10 °C/min: (a) cooling, and (b) heating.

has become amplified when vertical scale expansion was used to normalize the different scans. Table I summarizes the melting and crystallization peak positions for DMS-4-10 and 12. The extremely low crystallization temperature for DMS-5 was reproducible.

Figure 2 shows the thermal transition temperatures vs. flexible spacer number, n, for HMS-n and DMS-n. During cooling, HMS polycarbonates (Fig. 2a) show an isotropic-to-nematic transition (open squares) followed by a crystallization exotherm for the nematic-to-crystal transition (open circles). During heating, broad complex multiple melting endotherms are seen[1,2] and only the uppermost melting peak temperature for the crystal-to-isotropic transition ($k \rightarrow i$) is plotted in Figure 2a (solid circles). For HMS-n, the transition temperatures do not show much variation with flexible spacer, when the flexible spacer number ranges from $n = 4$ to 8. For $n > 8$, all transition temperatures drop.

TABLE I

Thermal Transition Peak Temperatures for DMS Polycarbonates at 10 °C/minute Scan Rate

Sample n	Crystallization Temp. (°C) T_c	Melting Temp. (°C) T_m
4	149	172
5	66	115
6	157	174
7	110	142
8	113	139
9	77	105
10	77	106
12	80	112

The DMS transition temperatures from DSC analysis are shown in Figure 2b. No isotropic-to-nematic transition was observed in any of the DMS polymers. In Figure 2b the crystallization peak temperatures during cooling (open circles) and the uppermost melting peak temperature during heating (solid circles) are shown. The odd-even effect in the crystallization and melting peak temperatures is seen for $n = 4$–8. The transitions associated with even parity flexible spacer are greater than those associated with odd parity. As with the HMS polycarbonates, in DMS-n all transition temperatures drop for $n > 8$.

Results of polarizing optical microscopy are shown in Figure 2c for DMS-n. POM was used to study the first appearance of birefringence during cooling (solid squares) and the final disappearance of birefringence during heating (open squares). For all samples except DMS-5, the temperatures shown in Figure 2c correspond very well with the DSC endothermic response shown in Figure 1. The first appear-

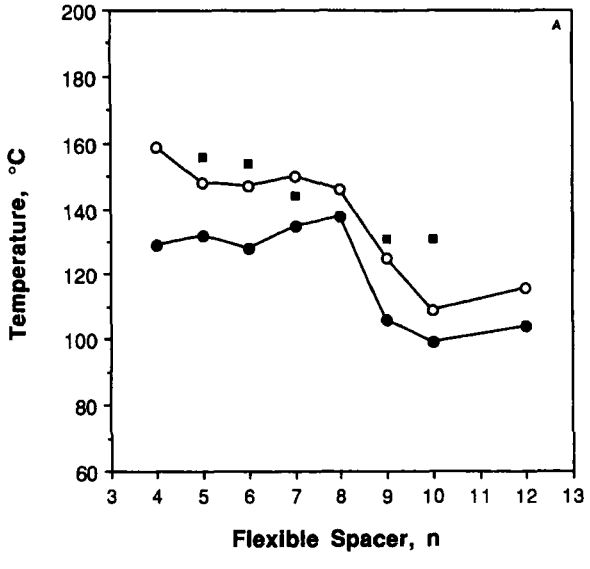

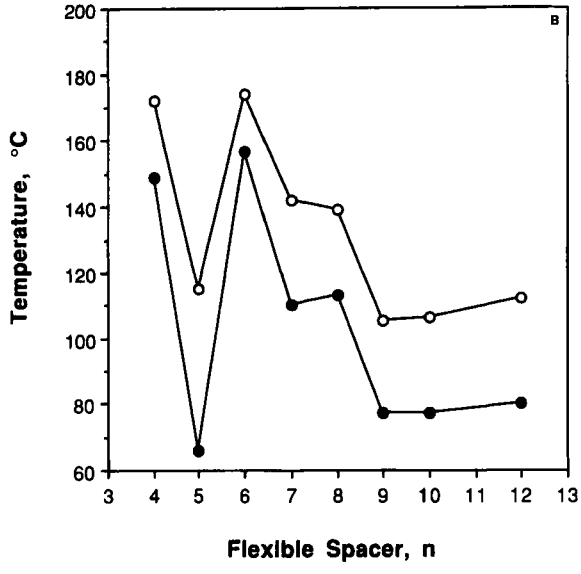

FIGURE 2

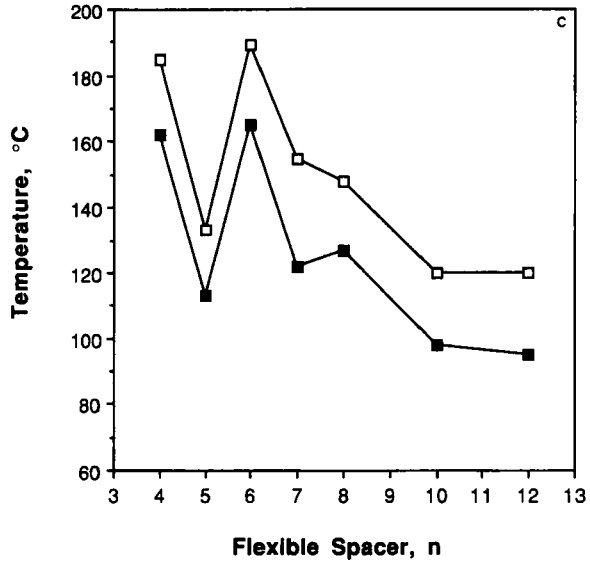

FIGURE 2 Thermal transition temperatures vs. flexible spacer number during cooling (solid symbols) and heating (open symbols). Lines are guides to the eye. (a) DSC data for HMS: $i \rightarrow lc$ (■), $lc \rightarrow k$ (○), $k \rightarrow i$ (○); (b) DSC data for DMS $l \rightarrow k$ (), $k \rightarrow i$ () (c) Birefringence data for DMS: First appearance of birefringence (■); disappearance of birefringence (□).

ance of birefringence closely matches the temperature of first departure of the exothermic peak during cooling. In DMS-5, large scale birefringence was observed to appear at 116 °C, whereas the DSC cooling scan revealed no exothermic departure from the baseline until 70 °C. The final disappearance of birefringence closely matches (again, except for DMS-5) the temperature at which the melting endothermic response is completed. As seen in Figure 2c, the birefringence temperatures also show an odd-even relationship with n for $n = 4-8$. The shape of the birefringence temperature curves is similar to the thermal transition temperature curves shown in Figure 2b. However, neither DSC nor POM revealed any isotropic-to-nematic transitions during cooling at 10 °C/min.

For the purpose of comparison, Figure 3a, b shows the cooling and reheating scans of DMS-7 and HMS-7. In both scans, the baseline of HMS-7 is tilted steeply

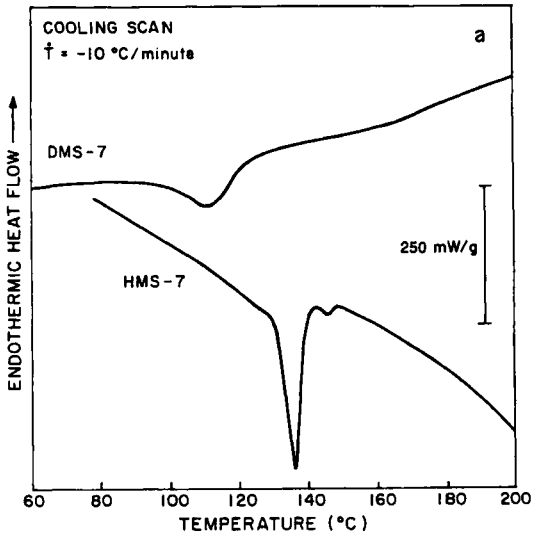

FIGURE 3

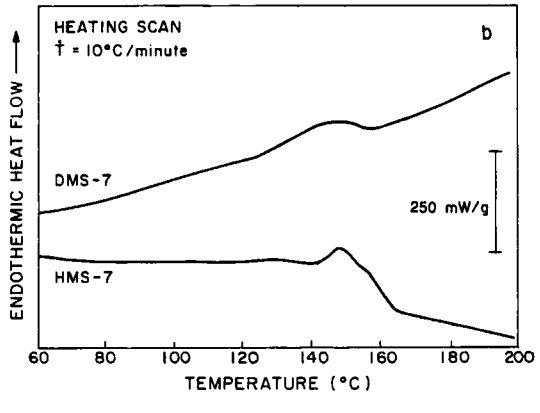

FIGURE 3 DSC thermograms of DMS-7 and HMS-7 at 10 °C/min: (a) cooling, and (b) heating.

down from left to right. DMS-7 has lower crystallization and melting temperature than HMS-7. In cooling, Figure 3a, DMS-7 shows a single broad exotherm. HMS-7 shows a double exotherm with a small, sharp isotropic-to-nematic (T_{i-lc}) transition followed by a much larger, sharp nematic-to-crystalline (T_{lc-k}) transition.

Figure 4a, b shows DSC cooling scans at various cooling rates for DMS-7 and HMS-7, respectively. DMS-7 has a single broad exotherm for all rates. HMS-7 has a large sharp exotherm followed by a broad low temperature tail at all rates. In addition, for rates of 10 °C/min or higher, the isotropic-to-nematic (T_{i-lc}) transition is seen clearly on the high temperature side of the main exotherm. As described previously[2], HMS-7 has a monotropic liquid crystalline phase, which can be observed in cooling only provided that the crystallization process is suppressed, for example, by increasing the cooling rate. The small higher temperature exotherm seen in Figure 4b represents the isotropic-to-liquid crystalline phase transition, T_{i-lc}, whose position is less affected by the cooling rate, compared with that of the large lower temperature crystallization exotherm. Therefore, at a slow cooling rate like 2 °C/min, the isotropic to liquid crystalline phase transition is covered by the crystalline phase transition. But at higher cooling rates, the liquid crystalline transition can be observed for HMS-7. In contrast, for DMS-7 shown in Figure 4a, higher cooling rates up to 50 °C/min still cannot separate the liquid crystalline transition from the crystalline phase transition.

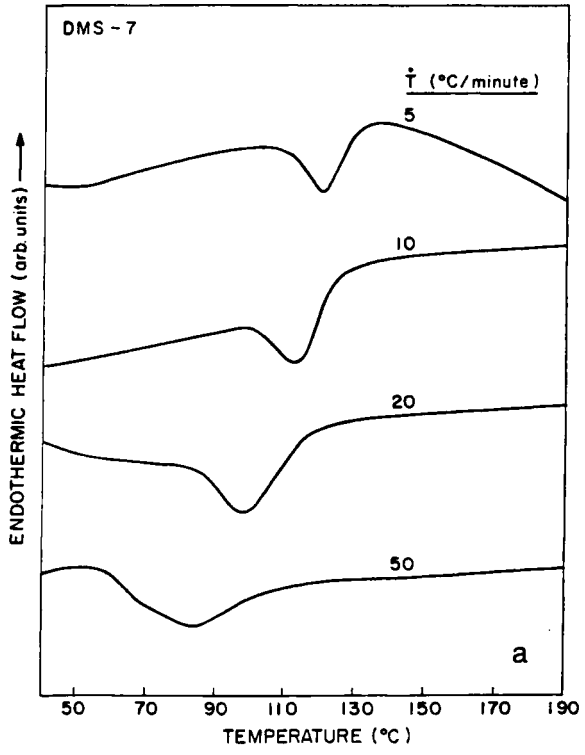

FIGURE 4

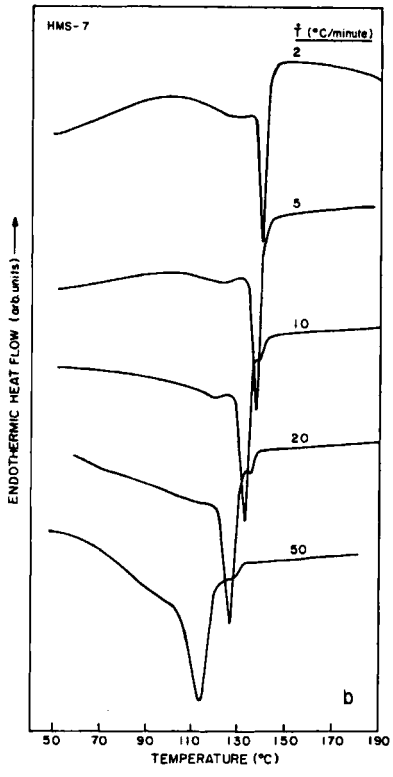

FIGURE 4 DSC thermograms of (a) DMS-7 and (b) HMS-7 at various cooling rates.

In the DSC isothermal crystallization study, the time to maximum heat flow at several crystallization temperatures, T_c, is obtained for DMS-7 and HMS-7, as shown in Figure 5a, b, respectively. The crystallization temperatures are lower for DMS than for HMS polymers, so the range of T_c's was chosen to give approximately the same rate of crystallization for comparison. The time to maximum heat flow of DMS-7 is less sensitive to the crystallization temperature increase than that of HMS-7. The relationship between the observed DSC melting point, T_m, and the crystallization temperature is found from the Hoffman-Weeks equation[21] as:

$$T_m = T_m^0(1 - 1/\gamma) - T_c/\gamma \tag{1}$$

where T_m^0 is infinite crystal melting point and γ is the thickening factor of the crystal lamellae. HMS-7 and DMS-7 have similar values of thickening factor and infinite crystal melting point as shown in Table II.

3.2. Small Angle X-Ray Scattering

We show in Figure 6a, b the Lorentz corrected SAXS intensity (Is^2) versus s data at room temperature of DMS-7 and HMS-7, respectively, which had been cooled at

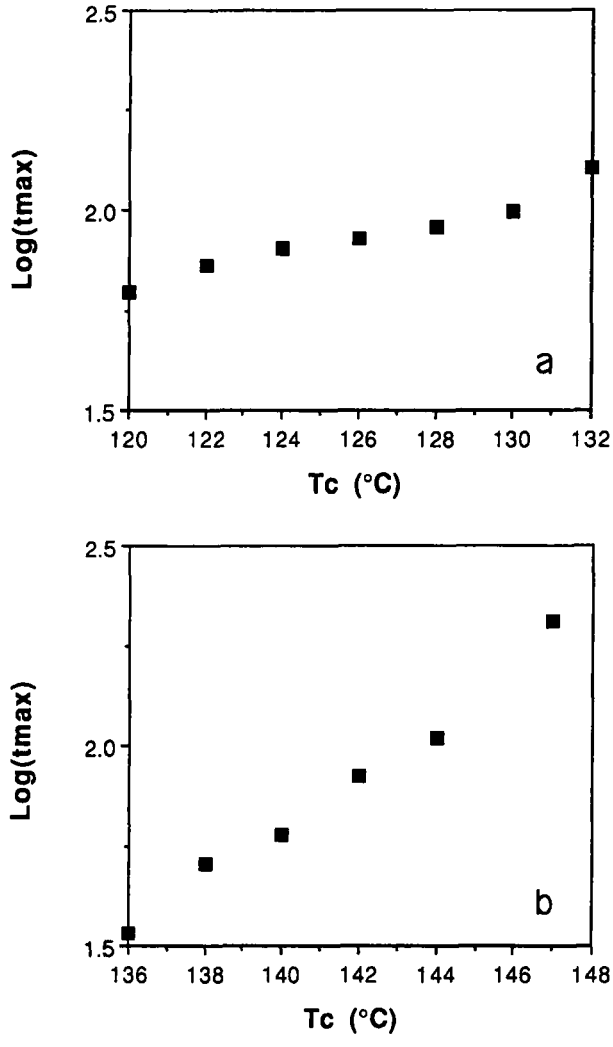

FIGURE 5 The time to maximum heat flow vs. crystallization temperature of: (a) DMS-7, and (b) HMS-7.

5 °C/min from the melt to room temperature. Considering that spherulites have been observed by optical microscopy[1], we assume that DMS polycarbonates have a lamellar structure in which stacks of lamellae alternate with amorphous material. Then the one-dimensional electron density correlation function, $K(z)$, is obtained by discrete Fourier transform of the Lorentz corrected intensity as described previously[4]. z is a dimension along the normal to the lamellar stacks which have a stack periodicity, L, also called the long period. Long period, crystal thickness, l_c, and linear crystallinity within the stacks, χ_c, are obtained according to the method proposed by Strobl and Schneider[22].

In Table III, we list long period, linear crystallinity, and crystal thickness at room temperature for DMS-5 to 8 and crystallized by cooling at 5 °C/min from the melt to

TABLE II

Infinite Crystal Melting Point† and Thickening Factor† for HMS-7 and DMS-7

Sample	Infinite Crystal Melting Point, T_m° (°C)	Thickening Factor, γ
HMS-7	189	1.2
DMS-7	203	1.3

† Determined from the Hoffman-Weeks equation[21].

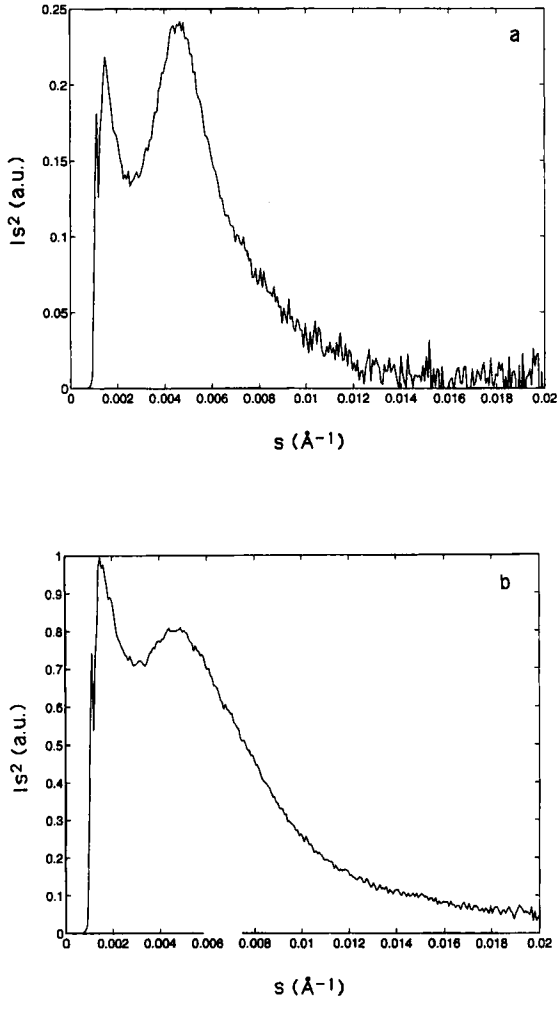

FIGURE 6 Lorentz corrected SAXS intensity, Is^2 vs. s at room temperature for (a) DMS-7 and (b) HMS-7, cooled at -5 °C/min from the melt.

TABLE III

Long period, Linear Crystallinity and Crystal Thickness for DMS-5-8 and HMS-5-8 Crystallized by Cooling at 5 °C/min from the Melt to Room Temperature

Sample	L(A) (±5A)	Xc (±0.01)	lc (A) (±2A)
DMS-5	230	0.20	32
DMS-6	189	0.28	45
DMS-7	218	0.29	67
DMS-8	191	0.28	47
HMS-5	214	0.26	44
HMS-6	215	0.21	33
HMS-7	234	0.25	46
HMS-8	230	0.18	29

room temperature. DMS-6,7 and 8 have similar values of linear crystallinity. But DMS-7 has higher value of crystal thickness and long period. With the exception of HMS-5, the HMS polycarbonates have higher values of long period, and lower values of linear crystallinity and crystal thickness than DMS polycarbonates with the same n number, HMS-5 reverses these trends compared to DMS-5. This is probably a result of the slower crystallization kinetics in DMS-5 which causes lower crystallization temperature and less perfect crystal structure, as shown in Figure 1 and Table I.

In Figure 7, we show Lorentz corrected intensity (Is^2) versus s data for the real time SAXS study of isothermal crystallization of DMS-7. The sample was melted and then cooled to 124 °C. The first scan at the bottom, marked $T = 154$ °C, is from the melt. The second scan from the bottom, marked $t = 0$, represents the initial stage of isothermal crystallization at 124 °C. Notice that by the time the cooling process from 154 °C to 124 °C is completed, significant intensity has already developed. Electron-dense phase formation does happen during the cooling process as DMS-7 is cooled through the isotropic to liquid crystalline transition. As described above, this $i \rightarrow lc$ transition can not be separated from the $lc \rightarrow k$ crystalline transition by thermal analysis. Also, from our DSC study of isothermal crystallization kinetics, we know the time to maximum exothermic heat flow is 81 seconds, for DMS-7 crystallized at 124 °C. The SAXS intensity shown in Figure 7 grows very fast before 81 seconds. Table IV shows the long period, linear crystallinity, and crystal thickness for DMS-7 and 8 isothermally crystallized at 124 °C without cooling. DMS-7 and 8 have similar values of linear crystallinity, crystal thickness, and long period.

The annealed HMS-7 and DMS-7 fibers display nice oriented fiber SAXS patterns (data not shown). The intensity maxima are located on the meridian and elongate in the direction of the equator, which is due to misorientation of the crystallites. The intensity of the meridian section is used to obtain linear crystallinity, crystal thickness and long period from the one-dimensional electron density correlation function for annealed DMS-7 and HMS-7 fibers, as listed in Table V. Annealed DMS-7 and HMS-7 fibers have similar values of crystal thickness, but DMS-7 has higher linear crystallinity and lower long period.

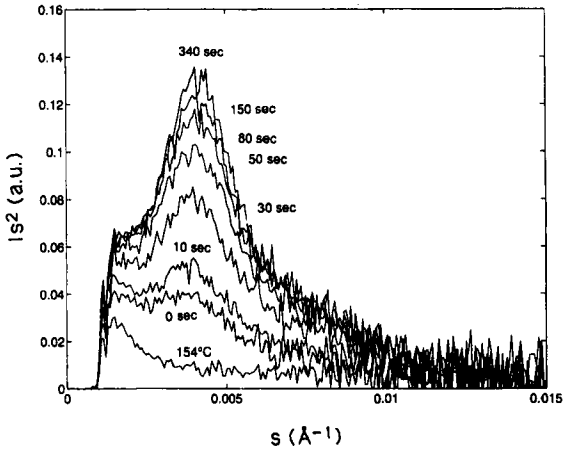

FIGURE 7 Real-time Lorentz corrected SAXS intensity, Is^2 vs. s Lowest curve marked 154 °C represents the melt state. Crystallization at 124 °C is recorded from $t = 0$ to $t = 340$ seconds.

TABLE IV

Long period. Linear Crystallinity and Crystal Thickness for Isothermally Crystallized Samples and Annealed Fibers

Sample	L(Å) (±5Å)	Xc (±0.01)	lc (Å) (±2Å)
	Isothermally Crystallized at 124°C		
DMS-7	245	25	55
DMS-8	251	24	53
	Annealed Fiber		
HMS-7	196	24	39
DMS-7	173	27	40

3.3. Wide Angle X-ray Scattering

Figure 8 shows WAXS reflection pattern of DMS-7 film, which was representative of the DMS-*n* polymers. The narrow single peak maximum located at d-spacing 4.4 Å suggests the existence of the nematic liquid crystalline order.

Figure 9a, b shows X-ray diffraction patterns of DMS-7 and HMS-7 raw fibers with fiber axis vertical. HMS-7 raw fiber X-ray diffraction pattern in Figure 9b displays two strong equatorial reflection (only one can be seen in the reproduction), which are associated with the (020) and (110) planes, as described in our previous publication[3]. Unlike HMS-7, DMS-7 raw fiber X-ray diffraction pattern in Figure 9a shows a diffuse ring with the maximum intensity on the equator. This pattern is similar to that of weakly ordered amorphous polymer, and indicates no strong orientation between adjacent DMS-7 polymer chains. Once the raw fiber is annealed, crystalline reflections are observed in both DMS-7 and HMS-7, as

TABLE V

Experimental and Calculated Crystallographic Parameters of a Crystal Unit Cell of DMS-7

Miller Index* (h k l)	2θ (°)		d-spacing (Å)	
	data	Calc.	data	Calc.
(1 1 0)	20.8(±0.3°)	20.9	4.3(±0.1Å)	4.2
(0 1 1)	10.4(±0.2°)	10.3	8.5(±0.1Å)	8.6
(0 2 0)	19.5(±0.2°)	19.5	4.5(±0.1Å)	4.6
(2 0 0)	36.6(±0.7°)	37.5	2.5(±0.1Å)	2.4
(0 1 2)	11.8(±0.2°)	11.9	7.5(±0.1Å)	7.4
(0 0 3)	10.2(±0.2°)	10.3	8.6(±0.1Å)	8.6
(1 3 0)	34.6(±0.5°)	35.0	2.6(±0.1Å)	2.6
(0 0 4)	13.8(±0.2°)	13.8	6.4(±0.1Å)	6.4
(1 2 4)	29.9(±0.5°)	30.4	3.0(±0.1Å)	2.9
(1 1 5)	27.0(±0. 3°)	27.3	3.3(±0.1Å)	3.3
(0 0 7)	23.4(±0.7°)	24.2	3.7(±0.1Å)	3.7

Miller indices are assigned based on orthorhombic structure with lattice parameters $a = 4.8$Å, $b = 9.1$Å, $c = 25.7$Å, $a = b = \gamma = 90°$

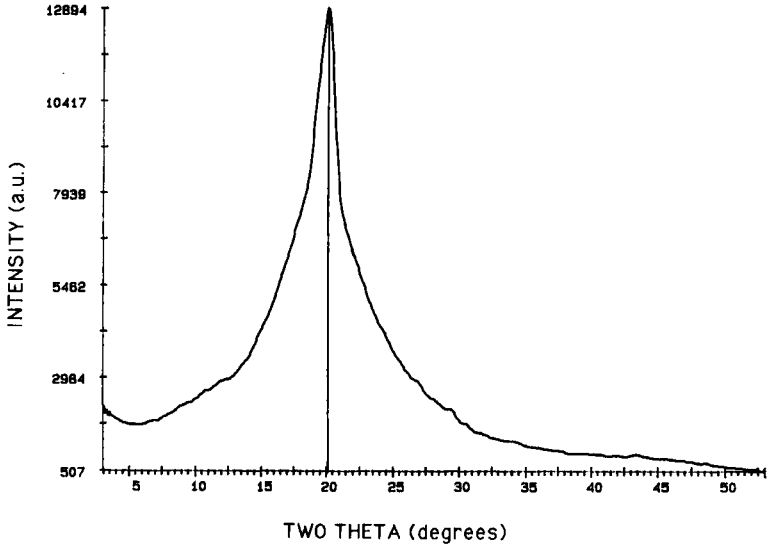

FIGURE 8 WAXS intensity versus two theta for DMS-7 in reflection mode.

shown in Figure 10a,b respectively. HMS-7 has a monoclinic crystal strucutre with $a = 9.4$ Å, $b = 7.9$ Å, $c = 25.6$ Å, $\alpha = 90°$, $\beta = 34.3°$, $\gamma = 90°$[3]. For DMS-7, an orthorhombic crystal structure with $a = 4.8$ Å, $b = 9.1$ Å, $c = 25.7$ Å, $\alpha = \beta = \gamma = 90°$, can be identified. The calculated scattering angle, 2θ, and corresponding d-spacings are shown in Table V, for direct comparison with the experimental data.

DMS-7 can be compared to an HMS polycarbonate having similar crystalline unit cell structure. Both DMS-7 and HMS-5 are orthorhombic. Notice in Table V that (00 *l*) reflections exist with l = odd in DMS-7 but no such reflections were seen in HMS-5[3]. Absence of (0 0 *l*) with l odd in HMS-5, is a signature of intermeshed structure in which adjacent chains are located at (0,0,0) and (1/2,1/2,1/2) positions. In DMS-7, existence of (0 0 *l*) for l odd indicates that this polymer does not have an intermeshed structure.

4. DISCUSSION

Effects of substitution on the mesogen have been reported by several groups[11,14,16]. Lenz[14] reports that "···even a slight change in the molecular structure of the mesogenic groups can result in significant change in the thermal properties of the mesophase". He attributed the decrease of the transition temperatures to steric hindrance by the substitutent, or interlocking of adjacent substituents. Two subsitutions of the same type affected the transition temperatures about twice as much as one substitution[14].

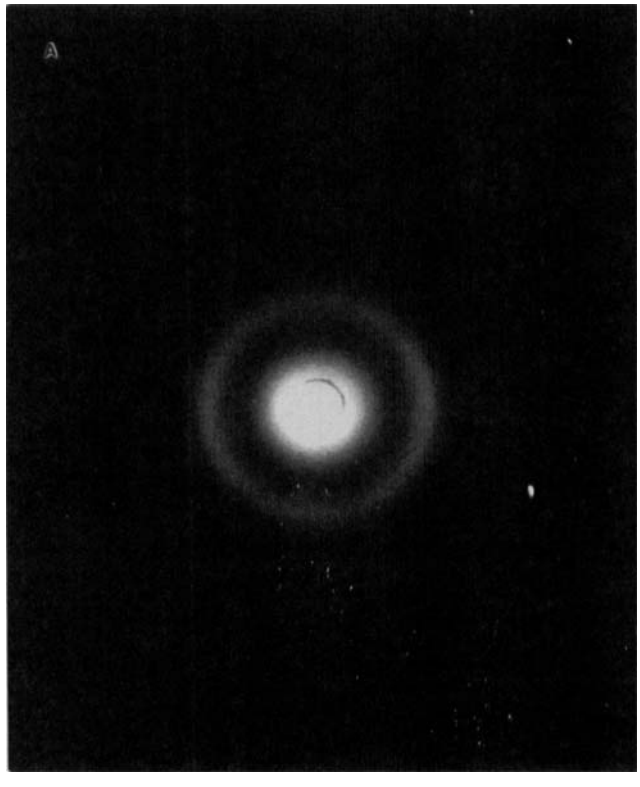

FIGURE 9

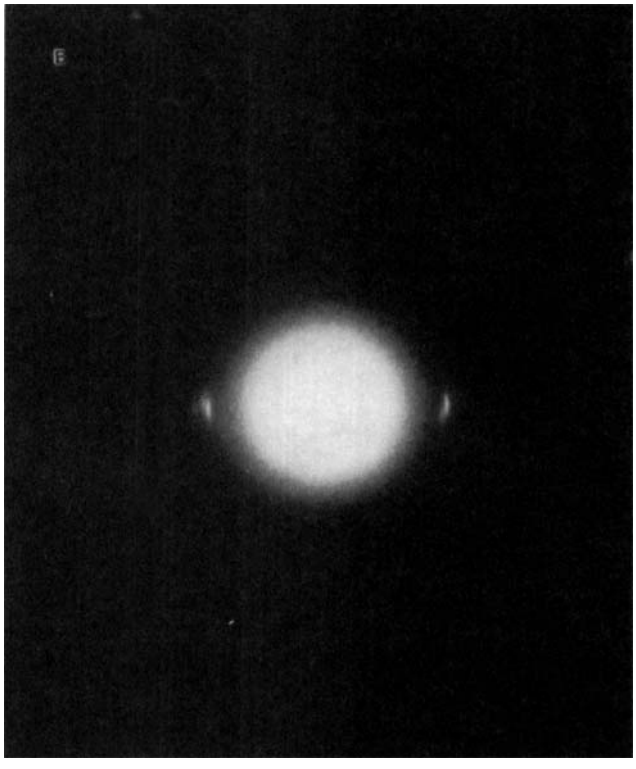

FIGURE 9 Flat film WAXS of hand drawn raw fibers in transmission mode: (a) DMS-7 and (b) HMS-7. Fiber axis is vertical.

Blumstein and coworkers[11] found that the ester group placement in azoxy polyester LCPs influenced the colinearity of the mesogenic core and extended spacer. Additionally, the transition temperatures dropped with the methyl substituent was ortho-linked (rather than meta-linked) to the nitrogens in the mesogen[11]. Roviello *et al.*[16] studied a stilbene-based polyester mono-substituted with CH_3. Compared to the unsubstituted mesogen, they saw no enantiotropic mesomorphism, and no monotropic mesomorphism down to 37 K below the melting temperature[16]. Thus, there is a precedent for observation of reduced transition temperatures with substitution on the mesogen, and the reduction in transition temperatures was greater with increased size of the subsitutent[14].

Considering our DMS and HMS polymers, the cross-section of the stilbene unit of DMS polycarbonates is 8.6 Å, whereas in HMS polycarbonates the cross-section is much smaller at 6.5 Å[1]. Therefore, we expect some differences in thermal behavior and mesophase stability between the two groups of polycarbonates due to steric packing differences. First of all, DMS polycarbonates have only one broad $i \rightarrow k$ exotherm, unlike HMS polycarbonates which show multiple exotherms, the uppermost of which reflects the $i \rightarrow lc$ transition. Also, in DMS polymers, the liquid

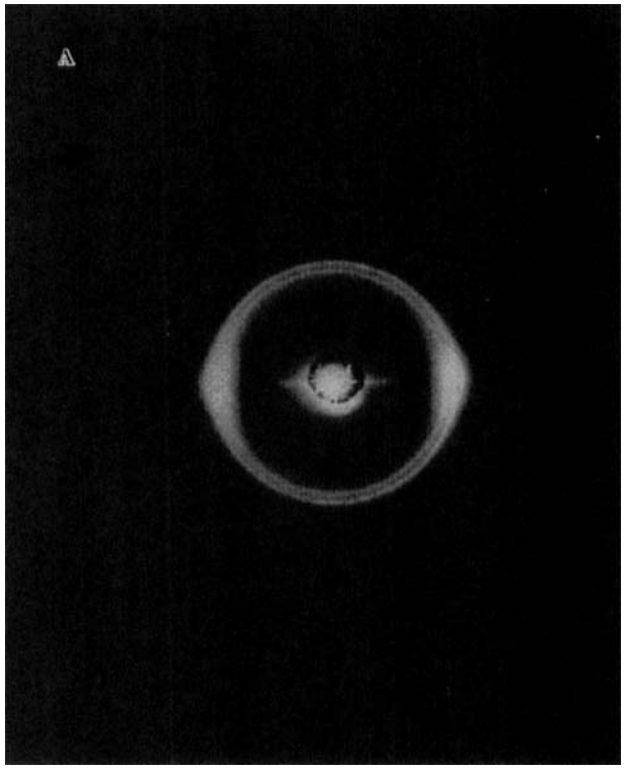

FIGURE 10

crystalline phase transition $i \rightarrow lc$ cannot be separated from the crystalline phase transition during cooling even at higher cooling rates. These facts suggest that DMS polycarbonates have less stable liquid crystalline phases than HMS polycarbonates. The second lateral substituent on the mesogen reduces the thermal stability of the liquid crystalline phase in DMS compared to HMS. This phenomenon has been observed in other LCPs[5,9,16]. The second lateral substituent on the mesogen separates the polymer chains further, which is also reflected in the larger crystal unit cell dimension for DMS-7 compared with HMS-7. The unit cell parameters relating to interchain distances are b and $a \sin\beta$ (where $\beta = 90°$ for DMS-7). The product of b and $a \sin\beta$ parameters gives the area of the basal plane (which is the plane perpendicular to the molecular chain axis). This area is 41.9 Å^2 for HMS-7, and 43.6 Å^2 for DMS-7, indicating that the unit cell of HMS-7 has chains more closely packed than the chains in DMS-7.

It is widely accepted that both the asymmetric shape and anisotropic molecular force are important to the stability of the liquid crystalline phase[23]. For DMS polycarbonates, not only the shape asymmetry but also the interaction between polymer chains is reduced. In Figure 11, a suggested Gibbs free energy diagram is shown schematically vs. temperature. The isotropic phase free energy, G_i, has the

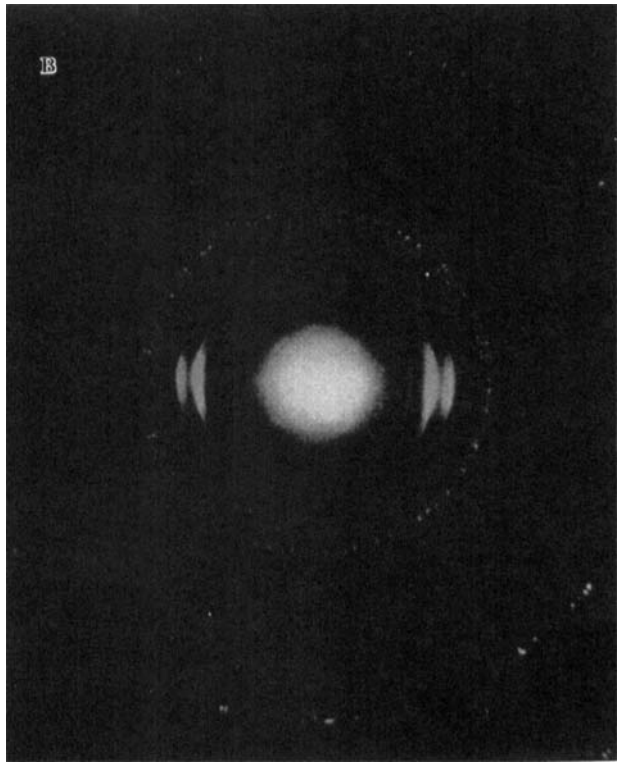

FIGURE 10 WAXS of hand drawn annealed fibers in transmission mode: (a) DMS-7 annealed at 125 °C and (b) HMS-7 annealed at 138 °C. Fiber axis is vertical. Spotty ring is from Si calibration standard.

greatest slope, reflecting greatest entropy. The crystalline phase free energy. G_k has the smallest entropy. The liquid crystalline phase free energies, for DMS (G_{lc-D}) and HMS (G_{lc-H}), are shown with the same entropy, intermediate between the isotropic phase and crystalline phase. As depicted in Figure 11, the free energy of the liquid crystalline phase for DMS polycarbonates is larger compared with HMS polycarbonates[24]. The transition temperatures from the isotropic phase to liquid crystalline phase are located at the intersection of G_i with G_{lc}. In this model, as a consequence of the higher liquid crystalline phase free energy of DMS compared with HMS, the T_{lc-i} of DMS polycarbonates (T_D) is pushed to even lower temperature and the virtual mesophase behavior is enhanced.

The times to maximum heat flow observed in the isothermal crystallization study are less sensitive to temperatures for DMS-7, compared with HMS-7. This result might also relate to the second lateral substituent on the mesogen. According to the kinectic theory of crystallization[21], the growth rate of crystals is proportional to $\exp(-K_g/T\Delta T)$, if crystallization happens in the temperature range of nucleation rate control. K_g is a parameter proportional to $1/\Delta f$, where Δf can be treated as the free energy difference between the crystalline phase and the liquid crystalline phase,

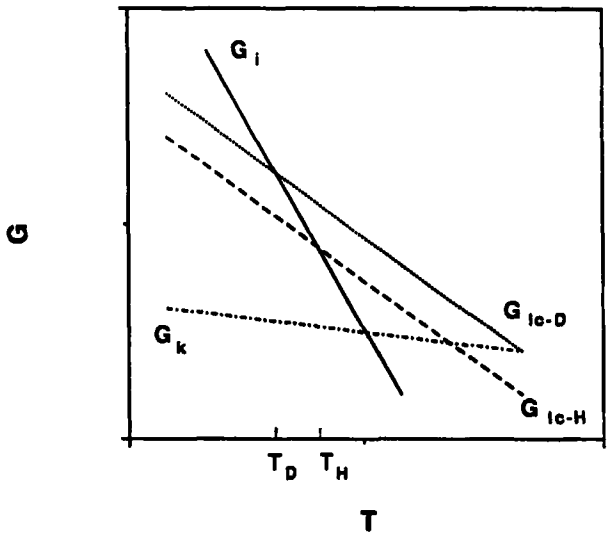

FIGURE 11 Schematic plot of Gibbs free energy vs. temperature: (- · -), G_k, crystalline phase; (—), G_i isotropic phase; (----), G_{lc-H}, liquid crystalline phase of HMS polycarbonates; and (·····), G_{lc-D}, liquid crystalline phase of DMS polycarbonates. The isotropic-to-liquid crystalline phase transition temperatures for HMS and DMS are indicated by T_H and T_D, the intersection temperatures of G_i with G_{lc-H} and G_{lc-D}, respectively.

which serves as crystal nuclei here. The growth rate of the HMS-7 crystalline phase is more sensitive to crystallization temperature change than the DMS-7 crystalline phase, which suggests that the Δf between the crystalline phase and the liquid crystalline phase should be smaller for HMS-7 than for DMS-7. This further supports our belief that the separation of adjacent DMS polycarbonate polymer chains lowers the stability of the liquid crystalline phase.

The closeness of adjacent polymer chains of HMS-7 compared to those of DMS-7 is also reflected in the raw fiber WAXS pattern. DMS-7 raw fiber pattern only shows a single diffuse maximum on the equator, which is characteristic of a nematic mesophase. However, HMS-7 raw fiber pattern displays two equatorial reflections, which reflects a higher level of order in the interchain packing.

DMS polycarbonates have odd-even property oscillation of thermal transition temperatures with the methylene spacer for $n = 4$–8, unlike HMS polycarbonates which show almost no dependence on n for $n = 4$–8. In the annealed fiber, DMS-7 does not exist in a stable intermeshed structure like HMS-7 does. It is our supposition that the steric effect of the second methyl substitution on the mesogen reduces the carbonate dipole interaction between adjacent polymer chains. DMS-7 and 8 seem to have close crystallization and melting transition temperatures. When DMS-7 and 8 are isothermally crystallized at 124 °C, they have similar values of linear crystallinity, crystal thickness, and long period. Though the crystal thickness and long period are higher for DMS-7 than DMS-8 when both are cooled at 5 °C/min from the melt, it is probably because a large population of less perfect crystalline lamellae are formed during the cooling process for DMS-8.

5. CONCLUSIONS

The steric effect of the second lateral methyl substituent on the stilbene mesogen lowers the stability of the liquid crystalline phase of DMS polycarbonates. Therefore, DMS polycarbonates only have a virtual liquid crystalline phase, unlike HMS polycarbonates which are able to form a monotropic liquid crystalline phase. Although both HMS and DMS polycarbonates are fast crystallizing materials, DMS polycarbonate crystallizes at lower temperature than HMS polycarbonate for comparable spacer length. DMS polycarbonates show odd-even property oscillation with the methylene spacer length.

Acknowledgements

Research was supported by U. S. Army Research Office (DAAH04-94-G-0317). Research carried out (in part) at the National Synchrotron Light Source, Brookhaven National Laboratory, supported by the U. S. Department of Energy, Division of Materials Science and Division of Chemical Sciences (DOE contact number DE-AC02-76CH00016). PPG Industries Foundation is acknowledged for supporting acquisition of the Silicon Graphics Workstation used for molecular modeling studies.

References

1. A. L. Bluhm, P. Cebe, H. L. Schreuder-Gibson, J. T. Stapler and W. Yeomans, *Mol. Cryst. Liq. Cryst.*, 239, 123 (1994).
2. Y.-Y. Cheng, P. Cebe, H. Schreuder-Gibson, A. Bluhm and W. Yeomans, *Macromolecules*, **27**, 5440 (1994).
3. Y.-Y. Cheng, M. Brillhart, P. Cebe, H. L. Schreuder-Gibson, A. L. Bluhm and W. Yeomans, *Mol. Cryst. Liq. Cryst.*, **270**, 61 (1995).
4. Y.-Y. Cheng, P. Cebe, M. Capel, H. Schreuder-Gibson, A. Bluhm and W. Yeomans, *J. Polym. Sci. Polym. Phys. Edn.*, **33**, 2331 (1995).
5. V. Percec, T. D. Shaffer and H. Nava, *J. Polym. Sci., Polym. Lett.*, **22**, 637 (1984).
6. A. Ruviello and A. Sirigu, *Makromol. Chem.*, **183**, 895 (1982).
7. A. Blumstein, *Polym. J.*, **17(1)**, 277 (1985).
8. C. Spies and H. G. Zachmann, *Am. Chem. Soc. Div. Polym. Chem. Polym. Propr.*, **36**, 318 (1995).
9. A. Sirigu, In *Liquid Crystallinity in Polymers: Principles and Fundamental Properties*, ed. by A. Ciferri, VCH Publishers, New York, 1991, Chapter 7.
10. J. Asrar, O. Thomas, Q. Zhou and A. Blumstein, *Proc. Macro-IUPAC*, Amherst, 1982.
11. A. Blumstein, S. Vilasagar, S. Ponrathnam., S. B. Clough, R. B. Blumstein and G.Maret, *J. Polym, Sci., Polym. Phys. Ed.*, **20**, 877 (1982).
12. B. W. Jo, R. W. Lenz and J. I. Jin, *Makromol. Chem. Rapid Commun.*, **3**, 23(1982).
13. R. W. Lenz, *Pure Appl. Chem.*, **57**, 1537 (1985).
14. R. W. Lenz, *Faraday Disc. Chem. Soc.*, **79**, 21 (1985).
15. K. Limura, N. Koide and R. Ohta, *Rep. Prog. Polym. Phys. Jpn.*, **24**, 231 (1981).
16. A. Roviello, S. Santagata and A. Sirigu *Makrmol. Chem. Rapid Commun.*, **4**, 281 (1983).
17. Q.-F. Zhou and R. W. Lenz, *J. Polym. Sci., Polym. Chem. Ed.*, **21**, 3313 (1983).
18. M. Sato, K. Nakatsuchi and Y. Ohkatsu, *Makromol. Chem., Rapid Commun.*, **7**, 231 (1986).
19. O. Glatter and O. Kratky, *Small Angle X-ray Scattering*, Academic Press.
20. J. T. Koberstein, B. Morra and R. S. Stein, *J. Appl. Cryst.*, **13**, 34 (1980).
21. J. D. Hoffman and J. J. Weeks, *J. Res. Natl. Bur. Stand.*, **66**, 13 (1962).
22. G. R. Strobl and M. Schneider, *J. Polym. Sci. Polym. Phys. Edn.*, **18**, 1343 (1980).
23. S. L. Kwolek, P. W. Morgan and J. R. Schaefgen, In *Liquid Crystalline Polymers, Encyclopedia of Polymer Science and Engineering;* Ed. by Jacqueline I. Kroschwitz, John Wiley & Sons, New York, 1985, vol 9.
24. V. Percec and A. Keller, *Macromolecules*, **23**, 4347 (1990).